

## Stretching, Unfolding, and Deforming Protein Filaments Adsorbed at Solid-Liquid Interfaces Using the Tip of an Atomic-Force Microscope

Douglas B. Staple,<sup>1</sup> Marko Loparic,<sup>2</sup> Hans Jürgen Kreuzer,<sup>1</sup> and Laurent Kreplak<sup>1,2</sup>

<sup>1</sup>*Department of Physics and Atmospheric Science, Dalhousie University, Halifax, NS, B3H 3J5, Canada*

<sup>2</sup>*M. E. Müller Institute for Structural Biology, Biozentrum, University of Basel, Klingelbergstrasse 70, CH-4056 Basel, Switzerland*

(Received 19 September 2008; published 27 March 2009)

Cells move by actively remodeling a dense network of protein filaments. Here we analyze the force response of various filaments in a simplified experimental setup, where single filaments are moved with an atomic-force microscope (AFM) tip against surface friction, with the AFM operating in the torsional mode. Our experimental findings are well explained within a simple model based on Newtonian mechanics: we observe force plateaus, which are the signature of the sequential stretching of single repeat units, followed ultimately by deformation of the whole polymer shape.

DOI: 10.1103/PhysRevLett.102.128302

PACS numbers: 82.37.Rs, 82.35.Gh, 82.37.Gk

During tissue morphogenesis, mammalian cells move within an extracellular matrix composed of cross-linked collagen fibrils [1]. The traction force enabling cell movement, typically several nN per  $\mu\text{m}^2$  [2], is localized at discrete sites called focal adhesions [3]. Such localized forces are sufficient to induce major rearrangements of the fibrillar elements [1,4]. These substrate changes are readily observable by atomic-force microscopy (AFM) of fibroblasts moving on glass coated with collagen fibrils: single fibrils appear bent, oriented in the direction of the closest cell adhesion site [5]. Here we develop a simplified experimental setup for analyzing the frictional and elastic response of fibrils: A single protein filament or fibril is adsorbed on a substrate and moved by an AFM tip perpendicular to the AFM cantilever axis and at a constant velocity [6]. The AFM cantilever twists substantially, generating force and moving the polymer forward [7].

Past studies addressing polymers on surfaces have classified adsorption regimes and behavior in the standard AFM geometry (retracting from the surface) [8]. Here we concentrate on the essential physics of manipulating molecules in the interfacial plane. We choose as model systems desmin intermediate filaments (IFs) and collagen fibrils; both adopt roughly linear configurations when adsorbed on mica (Fig. 1). The response of these two types of filaments to the AFM were qualitatively different: collagen fibrils were moved by the cantilever, elongated and bent into a continuous cusp shape [Fig. 1(b), arrow 1], while desmin filaments (and bundles of collagen fibrils) were locally stretched until broken, see Fig. 1(b) (arrow 2) and Fig. 2(a). These elongations imply that fibrils were locally stretched up to 3.5 and 1.3 times their original length, for desmin IFs and bundles of collagen fibrils, respectively. For both systems the stretching involved a few repeat units; however, for desmin this amounts to a length of  $\sim 150$  nm [Fig. 2(a)], whereas for the collagen bundles the deformed region was micrometers long [Fig. 1(b)]. To quantify these observations we show in Fig. 2(c) the force versus can-

tiliver displacement curves for a desmin filament. Such curves always show an initial linear region (in all of  $n = 60$  experiments), a force plateau, and a subsequent nonlinear increase in force [7]. In some experiments we observed two consecutive force plateaus, as shown in Fig. 2(c). Similar force curves with multiple steps were also observed for desmin filaments reassembled from a one-to-one mixture of wild-type desmin and a point mutant D399Y [9]; see Fig. 2(d). Because the torsional force constant of the AFM tips had to be relatively large to sustain forces up to  $f \approx 4$  nN, the resulting force fluctuations  $\delta f = (k_c k_B T)^{1/2} \approx 100$  pN are substantial, and must be filtered from the raw data; here we accomplish this filtering using a running-average over 5 nm.

The local stretching of filaments shown in Figs. 1 and 2 is an unexpected result considering their properties in solution. In solution fibrils appear rodlike on the  $\mu\text{m}$  scale, and these rodlike configurations are maintained during adsorption, as shown in Fig. 1(a). When stretched on the surface, however, these filaments form sharp “corners”

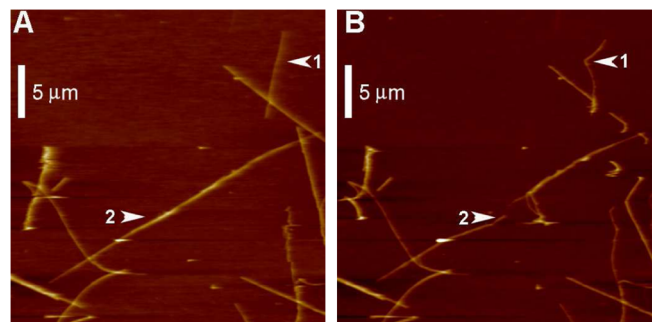


FIG. 1 (color online). Manipulation of collagen fibrils adsorbed to mica, pretreated with 1 M  $\text{MgCl}_2$  and immersed in PBS. Panels (a) and (b) were imaged prior to and after manipulation, respectively. Arrowheads identify two manipulations yielding a bent fibril with a cusped shape (1) and a stretched and broken bundle of fibrils (2).

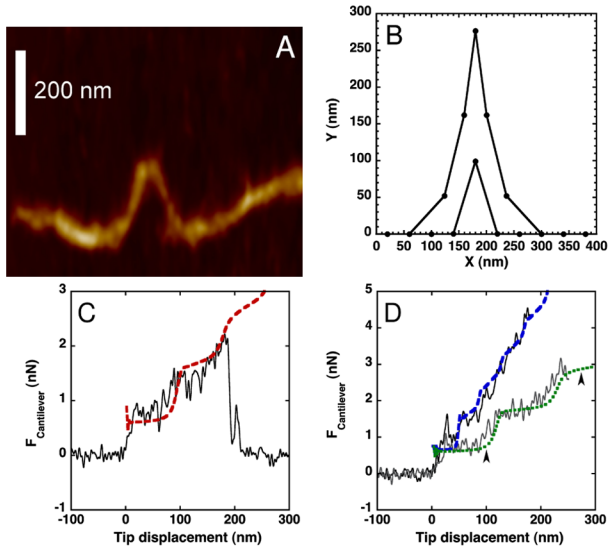


FIG. 2 (color online). (a) AFM image of single wild-type desmin filaments obtained after manipulation (adsorbed to mica and immersed in 25 mM Tris-HCl, 100 mM NaCl, pH 7.5). (b) Shape of a DC-WLC manipulated by a point probe at its middle for two cantilever displacements. (Dots represent beads and lines represent linkers.) Parameters:  $v = 50$  nm/s (as in experiment),  $L_p = 0.4$  nm,  $L_c = 3200$  nm,  $L_0 = 1000$  nm,  $N = 25$  beads, and  $N\nu = 0.3$  Ns/m. (c) Force versus displacement curves corresponding to panel A. Theoretical fit (broken line):  $L_c = 2200$  nm,  $N = 20$ , others as in panel (b). (d) Force versus displacement curves of desmin filaments containing an equal amount of wild-type proteins and mutant D399Y proteins [9] with theoretical fits. Arrowheads indicate tip displacements corresponding to the shapes presented in panel (b). Parameters (dotted curve): as in panel B; broken curve:  $L_p = 2$  nm,  $L_c = 1600$  nm.

and stretching continues in relatively straight subsegments [Fig. 1(a), arrow 2]. This implies that fibrils behave structurally different under these conditions; here the shape of the molecule is dominated by tension, rather than by bending rigidity as for solvated fibrils. In order to quantify these observations, we model filaments on surfaces as single or continuous-multistate wormlike chains (WLCs) subject to surface friction and external force. The fact that the filaments can be “stretched” implies that they have an effective contour length  $L_c$  longer than the end-to-end length with which they are adsorbed to the surface ( $L_0$ ). Furthermore, because we are stretching a small number of repeat units, we must account for the discreteness of the chain. To accomplish this we describe individual repeat units *separately*, using a WLC model for each segment. These separate WLCs are connected end-to-end to form the complete filament. Here we will refer to the individual WLCs as “linkers” and to the composite chain as a “discretely connected wormlike chain” (DC-WLC) [see Fig. 2(b)]. To simplify the inclusion of friction within a Langevin approach, we couple these massless linkers using beads with the mass  $m$  of a filament repeat unit. (In practice

the mass of the beads does not affect the results, as we are in the low Reynolds number limit.) This model is akin to the Rouse model, where we use WLC linkers instead of harmonic springs to account for the large effective extensibility of the chain ( $L_0 < L_c$ ). In summary, the filaments are modeled by  $N$  beads, connected by massless WLC linkers.

The motion of the polymer is controlled by the tension along the chain, the friction force on the molecule, and the force applied at some point along the chain by the AFM cantilever [see the inset of Fig. 3(a)]. For the tension on the  $i$ th linker we take the approximate force-extension relation of the WLC [10]:

$$f_i^{(t)} = \frac{k_b T}{L_p} \left[ \frac{1}{4(1 - x_i/L_b)^2} - \frac{1}{4} + \frac{x_i}{L_b} \right], \quad (1)$$

where  $T$  is the temperature,  $L_b = L_c/N$  is the contour length between beads, and  $x_i$  is the distance separating beads  $i$  and  $i + 1$ . The polymer remains in contact with the substrate during the whole experiment, and the  $i$ th monomer experiences a viscous drag or friction force, linear in the velocity of each monomer bead  $\mathbf{f}_i^{(f)} = -\nu \mathbf{v}_i$ , where  $\nu$  is the friction coefficient and  $\mathbf{v}_i$  is the velocity of the  $i$ th bead. In addition, the AFM tip exerts a force at a specific site of

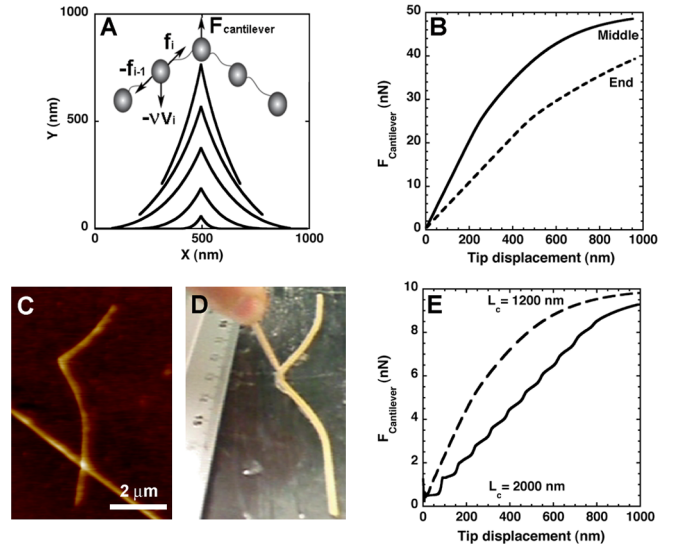


FIG. 3 (color online). Theoretical and experimental models. (a) Shapes of a DC-WLC chain manipulated by a point probe. Parameters:  $L_p = 1$  nm,  $L_c = 1200$  nm,  $N = 100$ ,  $N\nu = 1$  Ns/m, others as in Fig. 2(b). Inset: Schematic of the DC-WLC. (b) Force versus displacement curves for the same chain manipulated at its middle (solid line) and at one end (broken line). (c) AFM image of a collagen fibril after manipulation revealing a similar cusp shape. (d) A 12 cm long rubber band adsorbed to a glass plate coated with silicon grease (Corning) and manipulated at an average velocity of 3 mm/s. (e) Force versus displacement curves for two DC-WLC chains, with  $L_c = 1200$  and 2000 nm for solid, dashed curves, respectively. [ $N = 20$  beads; other parameters as in panel (a).]

the chain, e.g., in the middle or at one end,  $f_{i=a}^{(\text{AFM})} = k_c(vt - y_i)$ ; here we take the force to be due to a harmonic cantilever moving at a constant velocity. These forces are inserted into the Langevin equations for the individual beads, with the cantilever fluctuations as the external noise. The shape of the polymer chain as a function of time is obtained as the average motion, equivalent to the solution of Newton's equations. The role of the fluctuations will be studied elsewhere after appropriate measurements have been performed.

In our model the chain has an overall contour length  $L_c$  and is adsorbed to the substrate with an end-to-end length  $L_0 < L_c$ . Two cases are of interest:  $L_c \sim L_0$ , corresponding to collagen fibrils [11] and  $L_c \sim 2-3L_0$ , corresponding to desmin IFs [6]; this second case also encompasses other biopolymers such as DNA [12], and fibrin [13]. If the chain has a limited extension ( $L_0 \sim L_c$ ), or if the force necessary to extend the chain is small compared to the viscous drag  $\nu v$ , then the chain segments in the vicinity of the moving point probe extend first [Fig. 3(a)]. This process continues until all segments are under tension and gives rise to a linear force versus displacement curve [Fig. 3(b), solid line]. After all segments have extended close to their limit, the whole chain is set in motion [Fig. 3(a)] and the force converges asymptotically to  $\nu v$ . As expected, the force versus displacement curve depends on the position of the point probe along the polymers [Fig. 3(b), compare solid and broken lines]. The cusp shape of the chain is due to the incremental motion of chain segments nearest to the moving tip; this is observed both at the nano and macro scales, see Figs. 3(c) and 3(d). Indeed, we see the same cusped shape with rubber bands (mm scale) as with fibrils ( $\mu\text{m}$  scale).

For quantitative agreement between the model and experimental data, the viscous drag coefficient  $\nu$  had to be between  $10^{-3}$  and  $10^{-1}$  N s/m. Below  $10^{-3}$  N s/m the system is underdamped and strong oscillations occur; above  $10^{-1}$  N s/m the system is overdamped, and around  $10^2$  N s/m the chain is stuck to the substrate. In order to relate the viscous drag coefficient to a bulk viscosity  $\eta$ , we use Stokes's relation,  $\nu = 6\pi\eta a$ , where  $a$  is the radius of the particle. This radius can take any value between 1 and 100 nm for biopolymers, so our range of  $\nu$  is equivalent to a bulk viscosity  $\eta$  between  $10^3$  and  $10^7$  Pa s, corresponding to peanut butter and pitch, respectively. Although the AFM experiments are performed in water (bulk viscosity  $10^{-3}$  Pa s), the binding of the protein filaments to the substrate ions gives rise to an extremely viscous interface. These numbers compare well with estimates based on the thermal activation model by Briscoe and Evans [14,15] and also with estimates based on the Tomlinson model [16]. Because the equivalent viscosity is so high, the repeat units of the chain are stuck in position if no force is applied by the point probe. This is in agreement with the AFM experiments, where no evidence of relaxation was detectable

long after a given manipulation [7]. Even though we are studying a dynamic process, the large viscosity imposes a near-equilibrium stretching of the chain, validating the use of Eq. (1) to estimate the tensions at the linkers' ends.

For desmin filaments the number of participating repeat units is small because each unit can extend to several times its original end-to-end length before the next repeat unit is affected. We can account for this in the model by setting  $N$  to a small number; in such a situation the stretching of *individual* repeat units is observable as steps in the force versus displacement curve, if the units are extensible enough [Fig. 3(e), compare  $L_c = 1200$  nm and 2000 nm with 20 beads]. In addition, the deformation only affects the chain in the vicinity of the applied force, in stark contrast to the cusplike shape and in perfect agreement with experiment. (It should be noted that, when pulling in the center of a symmetric chain, one force step corresponds to *two* repeat units unfolding on opposite sides of the point probe.) So far, single force steps have been reported experimentally for desmin IFs [7] but not multiple ones. In these earlier experiments, the pieces of filament that were manipulated had an average length of only  $80 \pm 27$  nm ( $n = 60$ ) and the maximal tip displacement was on average  $150 \pm 41$  nm ( $n = 60$ ) [7]. Assuming in our model that each linker is 45–50 nm long and can extend to 160–180 nm maximum, the observation of more than one force step is indeed very unlikely. However, we did find, retrospectively, one force curve out of 60 measured in that study that displayed two force steps [7].

As further experimental evidence for the existence of multiple force steps in desmin filaments, we performed an additional  $n = 90$  experiments on a population of desmin filaments reassembled from a one-to-one mixture in urea of wild-type desmin and a point mutant D399Y [9]. AFM measurements were performed exactly in the same conditions as wild-type desmin filaments [7]; the pieces of filament that were manipulated had an average length of  $125 \pm 37$  nm ( $n = 90$ ), and the maximal tip displacement was on average  $215 \pm 73$  nm ( $n = 90$ ). As predicted by our model, we found samples with multiple force steps, as previously presented in Fig. 2(d). Such multiple steps were visible in a total of 11 out of  $n = 90$  curves; even though each individual curve was distinct from the others, it was possible to fit each one by allowing variations in the number of beads  $N$ , the contour length of the linkers  $L_c$ , and the persistence length  $L_p$ . Since we have to change the chain parameters ( $N$ ,  $L_c$ ,  $L_p$ ) to fit the experimental data, desmin filaments cannot be well modeled by a single DC-WLC. This is due to the fact that desmin IFs have a hierarchical structure, with around 40 protein chains arranged in parallel in the cross-section of the filament [9]. The chains dimerize to form 45 nm long repeat units, which are double stranded  $\alpha$ -helical coiled coils, and which can unfold upon stretching [17]. The unfolding of the coiled-coil essentially implies that the length of a

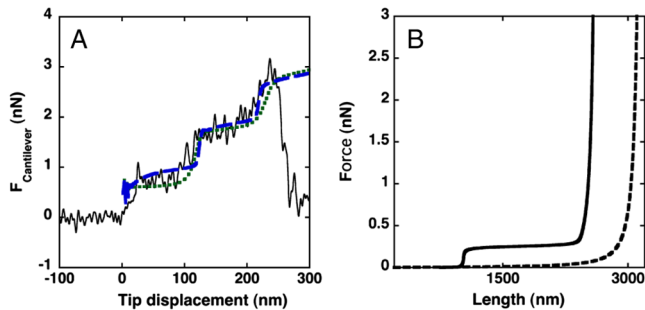


FIG. 4 (color online). (a) Comparison of the DC-WLC fit of Fig. 2(d) (dotted line) with a two-state model fit (broken line) for the same experimental curve. (b) equilibrium stretching curves for the two models: two-state (solid line) and DC-WLC (dotted line).

repeat unit increases. Sliding between the chains can also occur, explaining the extreme extensibility of these filaments [6]. Hence, the WLC linkers should be replaced by a more complex multistate polymer model.

As a step in that direction we have implemented a continuous two-state model for the linkers [18]: we describe the linker as a double stranded  $\alpha$ -helical coiled coil, 40 nm in length, composed of 0.15 nm long units that can unfold to 0.38 nm. The coiled-coil and unfolded polypeptides have persistence lengths of  $L_{p1} = 25$  nm [17] and  $L_{p2} = 0.4$  nm, respectively. We assume a Gibbs free energy difference between the two states of  $\Delta V = 250$  meV and an interaction energy between the two states of 20 meV, with other parameters as in Fig. 2(b). In Fig. 4(a) we show again the experimental data and corresponding fit from Fig. 2(d) (green dotted curve), which we compare with a fit from the two-state model [4(a), blue dashed curve]. Note that our original fit based on the simpler DC-WLC model is already within the experimental error; additional experiments are necessary to resolve the difference between the two fits. Nevertheless, this example demonstrates the potential of the techniques presented in this paper: Based on the fit parameters we can calculate the expected equilibrium force-extension relations in the standard AFM geometry (one end of the molecule tethered to the AFM tip); see Fig. 4(b). With the continuous two-state model we obtain a plateau force at 230 pN; this value is higher than the plateau forces measured for a single myosin coiled-coil [17], but desmin IFs consist, in cross-section, of around 20 coiled-coils wrapped around each other. Interestingly, assuming a filament diameter of 10 nm, the stress at the plateau is expected to be on the order of 3 MPa, which is in excellent agreement with published values for macroscopic bundles of IFs [19].

In summary, AFM manipulation of protein filaments at solid-liquid interfaces yields information about their mechanical properties relevant for the understanding of cell motion. In this study the AFM is moved perpendicularly to

its axis: torsional forces balance frictional and mechanical forces between the AFM tip and the molecule and surface. The mechanical properties of the stretched molecule are still visible in this geometry, and we observe the sequential unfolding of single repeat units as force plateaus. Differences in the mechanical response for different filaments can be traced back to their characteristics, namely, their contour length, their persistence length, and their friction coefficient. We demonstrate these features within a simple mechanical model, which is sufficient to understand the current experimental data.

This work was supported by grants from NSERC and the Office of Naval Research. D. S. would like to acknowledge NSERC and the Killam Trusts. M. L. would like to acknowledge an NCCR “Nanoscale Science” grant, awarded by the Swiss National Science Foundation to Ueli Aebi and Ivan Martin.

- 
- [1] D. Stopak, N. K. Wessells, and A. K. Harris, *Proc. Natl. Acad. Sci. U.S.A.* **82**, 2804 (1985).
  - [2] B. Sabass, M. L. Gardel, C. M. Waterman, and U. S. Schwarz, *Biophys. J.* **94**, 207 (2008).
  - [3] K. E. Kadler, A. Hill, and E. G. Canty-Laird, *Curr. Opin. Cell Biol.* **20**, 495 (2008).
  - [4] K. Wolf, I. Mazo, H. Leung, K. Engelke, U. H. von Andrian, E. I. Deryugina, A. Y. Strongin, E.-B. Bröcker, and P. Friedl, *J. Cell Biol.* **160**, 267 (2003).
  - [5] J. Friedrichs, A. Taubenberger, C. M. Franz, and D. J. Müller, *J. Mol. Biol.* **372**, 594 (2007).
  - [6] L. Kreplak, H. Bär, J. F. Leterrier, H. Herrmann, and U. Aebi, *J. Mol. Biol.* **354**, 569 (2005).
  - [7] L. Kreplak, H. Herrmann, and U. Aebi, *Biophys. J.* **94**, 2790 (2008).
  - [8] A. Serr and R. R. Netz, *Europhys. Lett.* **73**, 292 (2006).
  - [9] H. Bär, N. Mücke, P. Ringler, S. A. Müller, L. Kreplak, H. A. Katus, U. Aebi, and H. Herrmann, *J. Mol. Biol.* **360**, 1031 (2006).
  - [10] J. F. Marko and E. D. Siggia, *Macromolecules* **28**, 8759 (1995).
  - [11] Y. Lanir, *Biophys. J.* **24**, 541 (1978).
  - [12] C. Bustamante, J. F. Marko, E. D. Siggia, and S. Smith, *Science* **265**, 1599 (1994).
  - [13] W. Liu, L. M. Jawerth, E. A. Sparks, M. R. Falvo, R. R. Hantgan, R. Superfine, S. T. Lord, and M. Guthold, *Science* **313**, 634 (2006).
  - [14] B. J. Briscoe and D. C. B. Evans, *Proc. R. Soc. A* **380**, 389 (1982).
  - [15] J. N. Glosli and G. M. McClelland, *Phys. Rev. Lett.* **70**, 1960 (1993).
  - [16] C. Fusco and A. Fasolino, *Phys. Rev. B* **71**, 045413 (2005).
  - [17] I. Schwaiger, C. Sattler, D. R. Hostetter, and M. Rief, *Nature Mater.* **1**, 232 (2002).
  - [18] F. Hanke and H. J. Kreuzer, *Eur. Phys. J. E* **22**, 163 (2007).
  - [19] D. S. Fudge, K. H. Gardner, V. T. Forsyth, C. Riekel, and J. M. Gosline, *Biophys. J.* **85**, 2015 (2003).